articles

Measurements of relativistic time dilatation for positive and negative muons in a circular orbit

J. Bailey
Daresbury Laboratory, Warrington, Lancashire, UK

K. Borer
Physikalisches Institut, Universität Beon, Bern, Switzerland

F. Combley
Department of Physics, University of Sheffield, Sheffield, UK

H. Drumm
European Organization for Nuclear Research, Geneva

F. Krienen
European Organization for Nuclear Research, Geneva

F. Lange
Institut für Physik der Universität Mainz, Mainz, FRG

E. Picasso
European Organization for Nuclear Research, Geneva

W. von Ruden
Institut für Physik der Universität Mainz, Mainz, FRG

F. J. M. Farley
Royal Military College of Science, Shrivenham, Wiltshire, UK

J. H. Field
European Organization for Nuclear Research, Geneva

W. Flegel
European Organization for Nuclear Research, Geneva

P. M. Hattersley
Department of Physics, University of Birmingham, Birmingham, UK

The lifetimes of both positive and negative relativistic ($\gamma = 29.33$) muons have been measured in the CERN Muon Storage Ring with the results

$$\tau^+ = 64.419\ (58)\ \mu s, \quad \tau^- = 64.368\ (29)\ \mu s$$

The value for positive muons is in accordance with special relativity and the measured lifetime at rest: the Einstein time dilation factor agrees with experiment with a fractional error of 2×10^{-3} at 95% confidence. Assuming special relativity, the mean proper lifetime for μ^- is found to be

$$\tau_0^- = 2.1948\ (10)\ \mu s$$

the most accurate value reported to date. The agreement of this value with previously measured values of τ_0^+ confirms CPT invariance for the weak interaction in muon decay.

MEASUREMENT of the lifetime of a sample of radioactive material which is moving with a known velocity is a means of testing the so-called time dilation, or slowing down of moving clocks, predicted by the special theory of relativity. If, in addition the radioactive particles move in closed circular orbits then the conditions simulate those of the outward and return journey of the twin paradox in which, according to the theory, the journeying twin ages more slowly than the one who stays at home. In this situation it is also possible to search for any modification of the predictions of the theory due to acceleration.

A device which stores unstable elementary particles of high momentum is an excellent tool with which to carry out such measurements and here we report the results obtained with the Muon Storage Ring at CERN. Muons have a lifetime at rest of about 2.2 μs and decay into electrons neutrinos and anti-neutrinos

$$\mu^- \rightarrow e^- + \nu_\mu + \bar{\nu}_e$$

The decay electrons are readily detected. If the muon sample has a velocity v then the lifetime of the sample as measured in the laboratory is given by

$$\tau = \tau_0/[(1-(v/c)^2)^{\frac{1}{2}}] = \gamma\tau_0$$

where τ_0 is the lifetime for the particle at rest.

The previous Muon Storage Ring experiment at CERN reported[1] a value of the muon lifetime in flight for a relativistic factor $\gamma \simeq 12$, which agreed within 1% with the predicted value obtained by applying the above Einstein time dilation factor[2] to the measured lifetime at rest[3]. Here we report separate measurements for μ^+ and μ^-, with a γ factor of 29.33, which are an order of magnitude more precise and which show that the predictions of special relativity obtain even under accelerations as large as 10^{18} g and down to distances less than 10^{-15} cm.

In the latest Muon Storage Ring[4-9] muons of momentum 3.094 GeV/c ($\gamma \simeq 29.3$; $\beta = v/c = 0.9994$) circulate on orbits of 14 m diameter in a uniform magnetic field and a weak focusing electric quadrupole field[10]. The main purpose of the project was to measure the anomalous magnetic moment of the muon by observing the relative precession of its spin with respect to its momentum. The muons are born from pion decay

$$\pi^- \rightarrow \mu^- + \bar{\nu}_\mu$$

and by careful momentum selection in this process it is possible to obtain a circulating muon sample with high initial longitudinal polarisation. Decay electrons from the stored muons are detected in 20 shower counters inside the ring. By selecting only high energy electrons (forward going in the muon rest frame) it is possible to follow the muon spin precession since the decay electron distribution is assymetric with respect to the muon spin direction. The decay times are measured to high precision[11-13] so that the muon laboratory lifetime can be obtained by fitting the observed decay electron time spectrum which consists of an exponential decay modulated by the muon spin precession frequency (ω_a).

This spectrum is distorted by small systematic effects, however—notably the loss of muons from the trapping region before decay, the dependence of the background count rate,

and the variation of the decay electron detection efficiency as a result of gain changes during the muon storage period. The resulting modification to the normal modulated exponential decay spectrum may be expressed as

$$N(t) = N_0[1+SG(t)+F(t)]\{\exp(-t/\tau) \times \times [1-A\cos(\omega_a t+\varphi)]+B(t)\} \quad (1)$$

The functions $SG(t)$ and $F(t)$ represent the variation of detection efficiency and muon losses, respectively, while $B(t)$ is the background. For μ^- data the background is independent of time and at the negligible level of $\sim 2\times 10^{-5}$, but becomes more important in the μ^+ lifetime data owing to stored proton contamination. The minimisation and measurement of these systematic effects are discussed in some detail below.

Muon losses

The muons are injected by the decay in flight of 3 GeV/c pions inflected into the ring[4-9]. They initially fill the whole available phase space; however, particle loss involves preferentially those muon orbits which approach closest to the material limits of the storage region.

To reduce these losses we manipulate the muon orbits in the first few microseconds after injection (the rotation period of the muons is 0.147 μs) so that the muons which pass within ~1 cm of the walls are removed. The remaining muons are left in the central region of the aperture and have a much smaller probability of being lost. This 'scraping' is achieved by applying asymmetric voltages to the electrostatic quadrupoles[10] used to focus the particles. A vertical electric field shifts the median plane downwards, and simultaneously a horizontal electric field (outwards on one side of the ring, inwards on the other) shifts the orbit sideways. The muons of large betatron amplitude then strike appropriately located aperture stops. The scraping voltages are turned off with a time constant of 10 μs, allowing the muon population to return adiabatically to the centre of the storage region.

When a muon hits an obstacle it loses energy and has a high probability of emerging on the inside of the ring. The muon losses are therefore monitored by placing a detector against the vacuum chamber on the inside of the ring, in a position similar to that occupied by the decay electron detectors. The muon detector consists of a series of four scintillation counters each preceded by two-radiation-length lead converters. Muons are discriminated from electrons on the basis of pulse height. A 'muon' is defined as a particle which, for all four counters, gives a pulse height equivalent to that of a minimum ionising particle, the acceptance ranging from 50% below to 50% above this central value. Measurements in an electron beam show that for the relevant range of decay electron energies, this condition rejects electrons by a factor of ~700. The muon detector is used to optimise the n value of the focusing field for minimum muon losses, to test the scraping system, and to measure the loss correction $F(t)$.

In the optimum running conditions very few muons were lost after 100 μs. The above rejection ratio and the similarity in acceptance of the muon and electron detectors indicated that $\gtrsim 80\%$ of the 'muon' counts after this time were mis-identified electrons. This was confirmed with a small five-gap optical spark chamber placed behind the muon detector. Muons, identified by a straight track with four or five sparks, were found to form only 10% of the late time 'muon' counts.

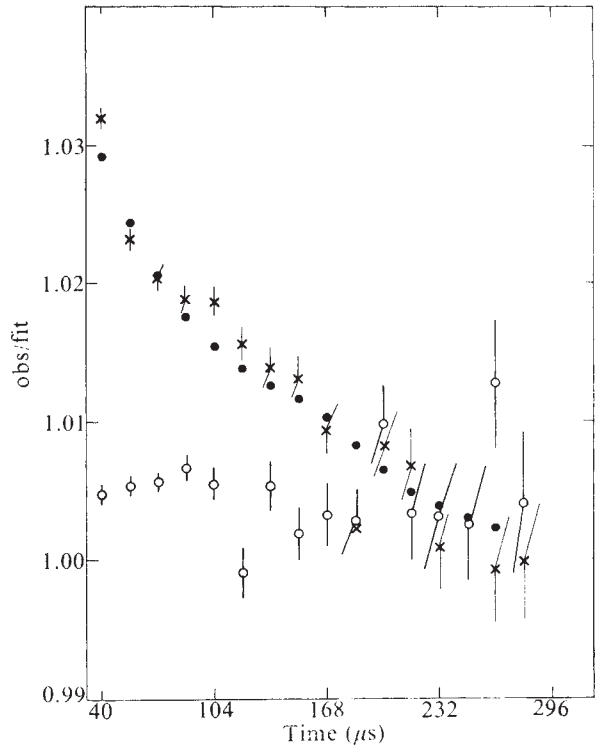

Fig. 1 Ratio of the decay electron time distribution (obs) to an exponential fit (fit) in the time range 300–650 μs. The g-2 modulation is included in the fit. The excess counts at early times over the extrapolated fit function show the effect of muon losses. ×, obs/fit no scraping. ●, Muon loss function as calculated from the muon detector time spectrum. ○, obs/fit with scraping.

The correction function $F(t)$ in equation (1) is given in terms of the lost muon time spectrum $M(t)$ (corrected for decay electron background) by the integral

$$F(t) = \frac{1}{\varepsilon\tau N_0}\int_t^{t_L} M(t)\exp(t/\tau)\,dt \quad (2)$$

where t_L is the end of the storage period and where the factor ε is the ratio of the detection efficiencies of the muon and electron detectors; its value and hence the absolute calibration of the muon detector is obtained as follows. In data where the losses are relatively high (those taken without scraping in operation), $F(t)$ can be deduced directly from the decay electron time distribution. Comparison with the values obtained from equation (2) provides the calibration of the muon detector and checks that it samples the lost muons in an unbiased way at different times.

This procedure and the effectiveness of the electric scraping are illustrated in Fig. 1. The points (a) represent the fractional

Table 1 Results for the muon lifetime in flight (μs)

Run	A	B	C	D	E	F
Charge of μ	+	+	—	—	—	—
Starting time of fit	100	100	50	50	90	100
Uncorrected lifetime (statistical error)	64.406 (66)	64.295 (103)	64.444 (55)	64.336 (36)	64.366 (84)	64.278 (60)
μ-loss correction	0.008 (8)	0.008 (8)	0.013 (8)	0.012 (8)	0.009 (8)	0.008 (8)
p-background correction	0.006 (2)	0.044 (22)	—	—	—	—
Gain correction	0.022 (20)	0.016 (20)	−0.010 (20)	−0.002 (20)	0.033 (20)	0.020 (20)
Fully corrected lifetime (total error)	64.442 (69)	64.363 (108)	64.447 (59)	64.346 (42)	64.408 (87)	64.306 (64)

Table 2 Lifetime results (μs)

	μ+	μ−	Weighted average μ+ + μ−
Lifetime in flight (this experiment)	64.419 (58)	64.368 (29)	64.378 (26)
Lifetime at rest (this experiment)	2.1966 (20)	2.1948 (10)	2.1952 (9)
Lifetime at rest (previous best measurements, refs. 18, 19)	2.19711 (8)	2.198 (2)	—

excess decay electron counts at early time with respect to a fit to the unscraped data at late time ($t > 300$ μs). Taking 40 μs after injection as $t = 0$, gives $F(0) = 0.03$ for these data. The points (*b*) are those calculated from the lost muon data, and the time dependence of these two data sets are in excellent agreement. The points (*c*) are the early time excess counts for the scraped data obtained in just the same way as (*a*). The calibrated muon detector gave a value $F(0) = 0.001$ in this case, so the loss level at 40 μs after injection is improved by a factor of ~30.

For the late starting times chosen in the analysis, the muon losses contribute at most a shift of 0.02% in the lifetime, as can be seen from the entries in Table 1.

Proton background

For the μ^+ data there is another complication in that the time-varying electric field associated with scraping enables protons to be stored in the ring. (The incident π beam is unseparated.) These protons are lost with a characteristic time distribution and so give background in both the decay electron and muon detectors. By assuming that the muon losses are the same for $\mu^\pm$ with identical machine parameters, the time distribution of these lost protons can (by subtraction) be found from the counts recorded in the muon detector. The relative detection efficiency of the muon and electron detectors for these protons is established in a separate experiment where the electric field is switched off ~1 ms after injection. At this time (~15.5 τ) only protons are stored, and the ratio of counts seen in the muon and the electron detectors directly gives the efficiency ratio. It turns out that the background level in the decay electron counts due to these 'unstable' protons is low ($\sim 3 \times 10^{-3}$ at 32 μs after injection) so the resulting correction to the lifetime is small, as shown in Table 1. The contamination of the μ^- data by stored antiprotons was at a negligible level.

Gain effects

The largest systematic effect which must be considered is the change in the energy acceptance of the decay electron detection system as a function of muon storage time. This effect is due to gain changes following the injection into the ring of one or more ~10 ns wide bunches containing $\sim 10^7$ particles (for more details of the effect of high particle flux on the gain of photomultipliers, see ref. 14); it is minimised by blanking off the dynode chain of the photomultiplier during, and for a few microseconds after, injection.

The system gain is measured as a function of time by means of light-emitting diodes (LEDs). The injected beam and all other conditions are the same as in normal data-taking. The signals from the LEDs are distinguished from decay electron counts by timing; a series of pulses are input to LEDs on the photomultipliers of the electron detectors at a number of fixed times throughout the muon storage interval. The output signal from each electron detector is split and input to two discriminators with a threshold separation of 3 dB. The LED pulse heights are adjusted so that all pulses fire the lower threshold discriminator and ~50% of the pulses fire the higher one, that is, the threshold of the latter is at the maximum of the LED pulse-height spectrum where the sensitivity to gain changes is greatest. A subsidiary calibration measurement of the pulse-height distribution for each LED-photomultiplier combination is made to establish the quantitative relation between the ratio of the counting rates output from the two discriminators and the gain change ΔG.

The gain curve is measured typically at 11 points between 7 and 580 μs for each counter, with a precision per point of ~0.1%. From the gain curves thus obtained, a counter selection is made to remove from the analysis counters with a steep gain variation. These counters are the ones which are struck preferentially by the injected beam. The mean gain curve of the remaining counters is typically flat to within ~0.1% over the whole muon storage interval. The mean gain curve $G(t)$ is multiplied by the factor $S \equiv \Delta N/(N\Delta G)$, the fractional change of counting rate of the decay electrons per unit gain change, to give the correction function in equation (1). For the electron energy threshold chosen for the lifetime analysis, $S = 1.00 \pm 0.02$.

The error in the gain correction was estimated by repeated measurement under identical running conditions. From the consistency of the slopes of mean gain curves measured at intervals of both a few days and several hours apart, this error is conservatively estimated to be ~0.03% in τ.

Results

Values of the muon lifetime in flight τ were found by fitting the experimental decay electron time distribution to the six-parameter function of equation (1) using the maximum likelihood method and varying the six parameters N_0, τ, A, ω_a, φ, B_0, where B_0 is the time-independent part of $B(t)$.

The results obtained for the lifetime for the two μ^+ and four μ^- runs which were separately analysed are presented in Table 1. The uncorrected lifetime, and the corrections with estimated systematic errors due to muon loss and gain effects, are shown for each run. In addition, for the μ^+ data, the proton background correction and error are shown. The starting times quoted for the fits vary from run to run as, according to the beam intensity used, the muon detector took varying times to regain full efficiency after injection. In all cases the upper limit of the time range of the fit is 650 μs.

The weighted average values of the lifetimes in flight for $\mu^\pm$ together with the combined average are given in the first line of Table 2.

Fig. 2 Bunch structure in the Muon Storage Ring from 6–10 μs after injection. Each bunch corresponds to one turn in the ring. Such distributions are analysed to give the mean rotation frequency $\bar{f}_{rot}$ of the stored muons, and hence the mean γ-factor $\bar{\gamma}$.

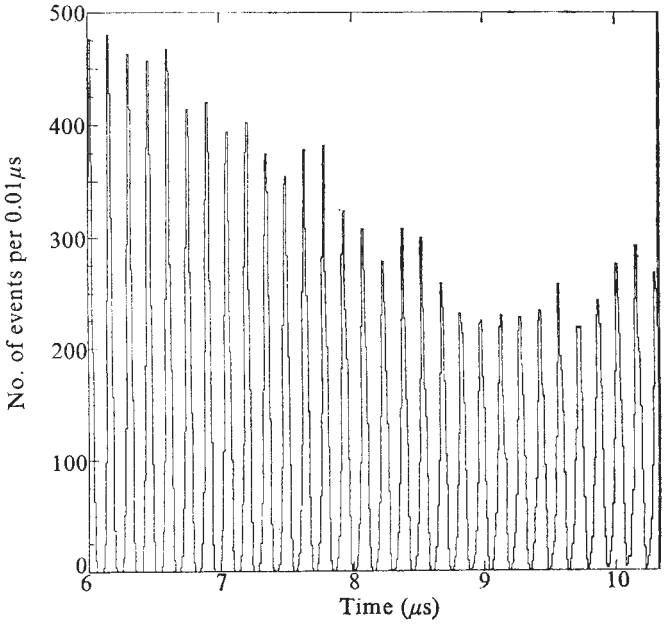

Table 3 Tests of relativistic time dilation from particle lifetime measurements. Values of $\tau_0 = \tau/\gamma$ are compared at different γ values

Particle	Refs	γ_1	γ_2	$[\tau_0(\gamma_1)-\tau_0(\gamma_2)]/\tau_0(\gamma_1)$ (%)	95% confidence limits (%)
$\pi\pm$	19–22	1.0	2.44	-2.5 ± 0.9	−4.3 to −0.7
$K\pm$	23, 24	1.0	3.38, 4.17	0.9 ± 0.3	0.3 to 1.5
K_S^0	25, 27	1.63	15.2	0.5 ± 0.6	−0.7 to 1.7
K_S^0	25, 26	1.63	20.2	0.2 ± 0.7	−1.2 to 1.6
μ^+	18 and this work	1.0	29.3	0.02 ± 0.09	−0.16 to 0.20

In the second line of Table 2 are given the corresponding lifetimes at rest τ_0 calculated using the Einstein[2] relation

$$\tau_0 = \tau/\gamma, \quad \gamma = [1-(v/c)^2]^{-\frac{1}{2}}$$

The average value of γ for the circulating muons is found by analysis[1] of the bunch structure of the stored muons (see Fig. 2) over a period of ~40 μs after injection. The mean rotation frequency $\bar{f}_{rot}$ is related to the average γ value $\bar{\gamma}$ by the expression

$$\bar{\gamma} = 2\lambda \bar{f}_p / g \bar{f}_{rot}$$

where $\bar{f}_p$ is the proton magnetic resonance frequency[15] (corrected to vacuum[16]) corresponding to the mean magnetic field, g is the g-factor of the muon, and $\lambda = \mu_\mu/\mu_p$ is the ratio of the muon and proton magnetic moments[17]. The result for $\bar{\gamma}$ is found to be

$$\bar{\gamma} = 29.327\,(4)$$

where the quoted error corresponds to an uncertainty of ±1 mm in the mean radius of the distribution of circulating muons.

The last line in Table 2 gives the most accurate published values for the μ^+ (ref. 18) and μ^- (ref. 3) lifetimes measured at rest. Comparing the high precision value of the μ^+ lifetime at rest, $\tau_0{}^+$, with the value found in this experiment we obtain

$$(\tau_0{}^+ - \tau^+/\bar{\gamma})/\tau_0{}^+ = (2\pm 9)\times 10^{-4}$$

At 95% confidence the fractional difference between $\tau_0{}^+$ and $\tau^+/\bar{\gamma}$ is in the range $(-1.6\text{–}2.0)\times 10^{-3}$. To date, this is the most accurate test of relativistic time dilation using elementary particles.

This result is compared in Table 3 with other limits on the validity of special relativity calculated from lifetime measurements given in the existing literature for $\pi^\pm$ (refs 19–22), $K^\pm$ (refs 23, 24) and K_S^0 (refs 25–27).

The entries in the table are the values of, and 95% confidence limits for $[\tau_0(\gamma_1) - \tau_0(\gamma_2)]/\tau_0(\gamma_1)$, where $\tau_0(\gamma_{1,2})$ are the lifetimes at rest as calculated via the Einstein relation using measurements on particles with mean γ values $\gamma_{1,2}$. The present experiment improves on the previously existing upper limits on violations of special relativity by about an order of magnitude.

The μ^+ measurement differs in one important respect from the other results quoted in Table 3. The $\pi^\pm$, $K^\pm$ and K_S^0 measurements in flight were performed in beams for which the decaying particle, regarded as a clock, was in an inertial (unaccelerated) frame. In the muon experiment, however, the particles are subjected to a constant transverse acceleration of 10^{21} cm s^{-2}. The muons perform a round trip and so when compared with a muon decaying at rest in the laboratory, simulate closely the so-called twin paradox which was already discussed in Einstein's first paper[2]. Other experiments[28,29] have confirmed the correctness of relativistic time dilation for clocks in circular motion to ~10% at low velocities (A similar conclusion follows from observations of the second-order (transverse) Doppler effect in the temperature dependence of the Mössbauer effect[23] and of the hydrogen maser frequency[24]). The present experiment is unique in its use of an ultra-relativistic clock ($\gamma \gg 1$) and its much greater precision ~0.1%.

The possibility also exists that very large accelerations may modify in some way the internal enstitution of particles[32–35]. No such effects, in so far as they affect the particle lifetime, are seen in this experiment where the transverse acceleration is $\sim 10^{18}$ g.

Some authors[36,37] have suggested that just as special relativity breaks down at very large distances owing to gravitational effects, there may also be a breakdown below some fundamental distance α. Rédei[38] has calculated the effect of such a breakdown on the muon lifetime in flight, and finds a γ^2 correction to the Einstein formula

$$\tau = \gamma\tau_0\,(1 + 2.5\times 10^{24}\,\gamma^2\alpha^2)$$

where α is in centimetres. From our value of τ^+ a limit can be set on α

$$\alpha \leqslant 9.6\times 10^{-16}\ \text{cm} \quad (95\%\ \text{confidence level})$$

Assuming the correctness of special relativity, the μ^- lifetime at rest $\tau_0{}^-$ given in Table 2 is the most precise value so far reported. Comparing this value with the high-precision measurement of $\tau_0{}^+$ it is found that

$$(\tau_0{}^- - \tau_0{}^+)/\tau_0{}^+ = -0.00105(46)$$

Or, at 95% confidence level, the fractional difference of $\tau_0{}^-$ and $\tau_0{}^+$ is in the range −0.002 to −0.00013.

The limit set on this quantity, which should vanish[39] by CPT invariance of the weak interaction, is comparable with that set by the best direct measurement[3] of the ratio $\tau_0{}^-/\tau_0{}^+$.

We thank all those who have contributed to this measurement of the muon lifetime. In particular, we thank F. Wickens for early calculations on the electric field configuration; E. M. McMillan for studies of various mechanisms of muon losses; R. W. Williams for analysis of the muon losses from the decay electron data; J. Lindsay for the preparation of a blanking scheme for photomultipliers and S. Wojcicki for his early contributions to the gain measurements.

Received 17 May; accepted 1 June 1977.

1 Bailey, J. *et al. Nuovo Cimento* 9A, 369 (1972).
2 Einstein, A. *Ann. Phys. (Germany)* 17, 891 (1905).
3 Meyer, S. L. *et al. Phys. Rev.* 132, 2693 (1963).
4 Bailey, J. *et al. Phys. Lett.* 55B, 420 (1975).
5 Combley, F. & Picasso, E. *Phys. Rep.* 14C, 1 (1974).
6 Farley, F. J. M. *Contemp. Phys.* 16, 413 (1975).
7 Field, J. H. *Proc. EPS Internat. Conf. High-Energy Phys.* Palermo, 1975, p. 247 (Editrice Compositori, Bologna, 1976).
8 Combley, F. H. *Proc. 7th Int. Symp. Lepton Photon Interactions at High Energies*, Stanford, 1975 (ed. Kirk, W. T.) p. 913 (SLAC, Stanford, 1975).
9 Bailey, J. *et al. Phys. Lett.* 68B, 191 (1977).
10 Flegel, W. & Krienen, F. *Nuclear Instrum. Meth.* 113, 549 (1973).
11 Pizer, H. I. *Nuclear Instrum. Meth.* 123, 461 (1975).
12 Pizer, H. I., van Köningsveld, L. & Verweij, H. *CERN* 76–17 (1976).
13 Field, J. H., Lange, F. & von Rüden, W. *Nuclear Instrum. Meth.* 143, 227 (1977).
14 Farley, F. J. M. & Carter, B. S. *Nuclear Instrum. Meth.* 28, 279 (1964).
15 Borer, K. *Nuclear Instrum. Meth.* 143, 203 (1977).
16 Borer, K. & Lange, F. *Nuclear Instrum. Meth.* 143, 219 (1977).
17 Crowe, K. M. *Phys. Rev.* D 5, 2145 (1972).
18 Balandin, M. P., Crebenyuk, V. M., Zinov, V. G., Konin, A. D. & Ponomarev, A. N. *Soviet Phys. JETP* 40, 811 (1974).
19 Nordberg, M. E., Lobkowicz, F. & Burman, R. L. *Phys. Lett.* 24B, 594 (1967).
20 Ayres, D. S. *et al. Phys. Rev.* D 3, 105 (1971).
21 Dunaitsev, A. F., Prokoshkin, Y. D., Razuvaev, E. A., Sergeev, V. A. & Simonov, Y. N. *Soviet J. Nuclear Phys.* 16, 292 (1973).

22 Ayres, D. S. *et al. Phys. Rev.* **157**, 1288 (1967).
23 Ott, R. J. & Pritchard, T. W. *Phys. Rev.* D **3**, 52 (1971).
24 Lobkowicz, F., Melissinos, A. C., Nagashima, Y. & Tewksbury, S. *Phys. Rev.* **185**, 1676 (1969).
25 Skjeggestad, O. *et al. Nuclear Phys.* **48B**, 343 (1972).
26 Geweniger, C. *et al. Phys. Lett.* **48B**, 487 (1974).
27 Carithers, W. C. *et al. Phys. Rev. Lett.* **34**, 1244 (1975).
28 Hay, H. J., Schiffer, J. P., Cranshaw, T. E. & Egelstaff, P. A. *Phys. Rev. Lett.* **4**, 165 (1960).
29 Hafele, J. C. & Keating, R. E. *Science* **177**, 166 (1972).
30 Pound, R. V. & Rebka, G. A., Jr *Phys. Rev. Lett.* **4**, 274 (1960).
31 Vessot, R. F. C. & Levine, M. W. *Metrologia* **6**, 116 (1970).
32 Sherwin, C. W. *Phys. Rev.* **120**, 17 (1960).
33 Romain, J. E. *Rev. mod. Phys.* **35**, 376 (1963).
34 Bailey, J. & Picasso, E. *Prog. Nuclear Phys.* **12**, 43 (1970).
35 Ageno, M. & Amaldi, E. *Academie Nazionali dei Lincei, Serie VIII*, VIII, Fascicolo I (1966).
36 Blokhintsev, D. I. *Phys. Lett.* **12**, 272 (1964).
37 Rédei, L. B. *Phys. Rev.* **145**, 999 (1967).
38 Rédei, L. B. *Phys. Rev.* **162**, 1299 (1967).
39 Lüders, G. & Zumino, B. *Phys. Rev.* **106**, 345 (1957).

Rifting and subsidence on passive continental margins in the North East Atlantic

L. Montadert
Division Geologie, Institut Francais du Petrole, 1.4 Av. de Bois-Preau, 92502 Rueil Malmaison, France

D. G. Roberts
Institute of Oceanographic Sciences, Wormley, Godalming, Surrey, UK

G. A. Auffret
Centre Oceanologique de Bretagne, CNEXO, 29.273 Brest, France

W. Bock
Rosentiel School of Marine & Atmos. Science, 4600 Rickenbacker Causeway, Miami, Florida 33149

P. A. DuPeuble
Universite de Rouen, Laboratoire de Geologie, Faculte des Sciences, 76130 Mont Saint-Aignan, France

E. A. Hailwood
Department of Oceanography, University of Southampton, Southampton, UK

W. Harrison
Oklahoma Geological Survey, University of Oklahoma, 830 van Fleet Oval, Norman, Oklahoma 73069

H. Kagami
Ocean Research Institute, University of Tokyo, Nakano, Tokyo 164, Japan

D. N. Lumsden
Department of Geology, Memphis State University, Memphis, Tennessee 38152

C. Muller
Geologisch-Palaontologisches Institut, Johann-Wolfgang-Goethe-Universitat, Frankfurt, Germany

D. Schnitker
Department of Oceanography, University of Maine, Walpole, Maine 04573

R. W. Thompson
Humboldt State University, School of Natural Resources–Oceanography, Arcata, California 95521

T. L. Thompson
University of Oklahoma, Department of Geology & Geophysics, Norman, Oklahoma 73069

P. P. Timofeev
Geological Institute, USSR Academy of Sciences, Pyzhevsky per 7, Moscow ZH 17, USSR

Deep-sea drilling in the Bay of Biscay and the Rockall Plateau show that passive continental margins are characterised by the absence of seismicity and include continental shelf, continental slope and continental rise physiographic provinces, exemplified by the borders of the Atlantic Ocean.

HYPOTHESES postulated for the structural and stratigraphical evolution of passive margins are based on the available geological and geophysical data, and analogies drawn with present day margins thought to represent stages in margin evolution[1–5]. In the initial stages, rifting of the continent perhaps contemporaneous with regional uplift takes place[6]. When the continental crust is completely rifted apart, ocean crust begins to accrete at the axis of the diverging plates. Heat dissipation[7] through the cooling continental and oceanic lithosphere is thought to result in subsidence, permitting transgression. The subsequent development of the margin depends on the variable roles in both time and space of subsidence, sediment loading, climate and ocean circulation. For example, the lithology and volume of sediments may be influenced by global transgressions and regressions[8,9], although their effects, in turn, depend on the altitudes of the continents and their rate of subsidence.

The relationship between the subsidence history, the rifting environment and the unconformities observed beneath many passive margins is, in particular, poorly understood because of a paucity of relevant deep sea drilling data. We report here some preliminary relevant results from the holes drilled on the passive margins of the Bay of Biscay and the Rockall Plateau during Leg 48 of the International Phase of Ocean Drilling (IPOD) of the Deep Sea Drilling Project (Figs 1, 2, 3).

The Bay of Biscay and Rockall Plateau

The northern margin of the Bay of Biscay[10–14] is comprised of the wide Celtic shelf and a broad continental slope that is dissected by many canyons and broken by the Meriadzek Terrace. Detailed multi-channel seismic surveys made by the Institute Francais du Petrole, the Institute of Oceanographic Sciences and the Centre National d'Exploitation des Oceans, show thin Tertiary and Cretaceous sediments overlying tilted blocks and half grabens that trend sub-parallel to the margin and control the relief of the Meriadzek Terrace (Fig. 2). Previous geological and geophysical studies have suggested that the Bay of Biscay was formed by rifting in Late Jurassic–Early Cretaceous time and by spreading during Early to Upper Cretaceous time[10–18]. However, the relation between the spreading and the subsidence history of the margin is not known. The three sites drilled in Biscay (Fig. 2) form a transect from the upper slope (site 402A) to the lower slope (site 400A) within 40 km of the continent–ocean boundary at the Trevelyan escarpment[18].

In contrast to the Bay of Biscay, three phases of rifting and spreading isolated the Rockall Plateau microcontinent and formed its margins[19–23]. The first opened the Rockall Trough in Early–Late Cretaceous time, and the second, in Late Cretaceous time (76 Myr), opened the Labrador Sea,